International Journal of Architectural, Civil and Construction Sciences
ISSN: 2415-1734
Vol:11, No:9, 2017

Thermal Modelling and Experimental Comparison for a Moving Pantograph Strip

Nicolas Delcey, Philippe Baucour, Didier Chamagne, Geneviève Wimmer, Auditeau Gérard, Bausseron Thomas, Bouger Odile, Blanvillain Gérard

***Abstract*—**This paper proposes a thermal study of the catenary/pantograph interface for a train in motion. A 2.5D complex model of the pantograph strip has been defined and created by a coupling between a 1D and a 2D model. Experimental and simulation results are presented and with a comparison allow validating the 2.5D model. Some physical phenomena are described and presented with the help of the model such as the stagger motion thermal effect, particular heats and the effect of the material characteristics. Finally it is possible to predict the critical thermal configuration during a train trip.

***Keywords*—**2.5D modelling, pantograph/catenary liaison, sliding contact, Joule effect, moving heat source.

I. Introduction

THE pantograph strip is one of the most problematic piece of a train. It is subjected to many physical phenomena which are especially unpredictable and often generate damage and thus lead to important maintenance works. To overcome this extra charge, an accurate study of the different kinds of wear has to be performed. This paper deals with one of them, namely the thermal wear.

From a general point of view, the strip temperature evolution is limited by two constraints. The first one is due to the material it-self. Indeed, the pantograph is often made in special carbon, matter which has been studied in [3], [7]. They show that the carbon wear thermal limit is around 400 °C. The second constraint comes from the glue used to fix the strip with its support. According to the manufacturer, this glue can't reach temperatures higher than 200 °C.

As provided, the strip wear is linked to its temperature, and thus to the fluxes and thermal productions applied to the system. Two kinds of heat production take part in a pantograph strip in motion. The first one is a volumetric heat production generated by the electrical field inside the strip. The second is a surface heat production which includes both Joule effects due to the contact area resistance (analytically studied in [2] and experimentally in [17]) and friction. The thermal fluxes acting in the strip are convection and conduction together with a storage effect. For more details on these fluxes, refer to [6].

N. Delcey is with the Femto-St Laboratory, Department of Energy, University of Bourgogne Franche-Comte, Belfort, France 90000 (corresponding author, e-mail : nicolas.delcey@femto-st.fr).

P. Baucour, D. Chamagne, G. Wimmer are with the Femto-St Laboratory, Department of Energy, University of Bourgogne Franche-Comte, Belfort, France 90000.

T. Bausseron is with the SNCF, Department of I & P, (Engineering & Projects), St-Denis, France 93200.

O. Bouger, G. Auditeau are G. Blanvillain are with SNCF, Department of CIM (Engineering Material Center), Le Mans, France 72100.

As the train is moving, the catenary wire which ensures power supply is also moving along the x-axis (see Fig. 1) on the strip's top surface. This phenomena is induced by a zig-zag positioning of the catenary wire (*i.e* the wire is never strictly parallel to the railway).

Such a system has already been studied in several specific cases. In [14] the strip overheating in motionless situation is highlighted and in [13] the impact of strip material on the temperature rise is proposed. Paper [15] deals with temperature effects on the strip wear, according to velocity and contact force, via a test bench. However, despite the large studies panel considered, we haven't found a real numerical approach for trains in motion.

In this paper, we present a thermal numerical simulation model of the strip as the train is in motion. However, for industrial issues, this model needs to be fast, accurate and economical from a computer memory point of view. So, some mathematical and numerical processes have been used to reach theses criteria.

The resulting model is a 2.5D dimensionally model *i.e* a 1D model in one direction (x) coupled to a 2D model in the two other directions (y-z). The resulting program allows visualizing thermal critical phases in function of the multiple inputs and predict the wear rate and thus anticipate maintenance operations.

II. System Presentation

A pantograph strip is often composed of impregnated carbon with copper. The thermal characteristics such as the thermal conductivity k [$\mathrm{W \cdot m^{-1} \cdot K^{-1}}$], the heat capacity C_p [$\mathrm{J \cdot K^{-1} \cdot kg^{-1}}$] or the density ρ [$\mathrm{kg \cdot m^{-3}}$] are given by the strip supplier. The convective coefficient is denoted h [$\mathrm{W \cdot m^{-2} \cdot K^{-1}}$]. The volumetric and surface heat production are defined by $\dot{Q}_v$ [$\mathrm{W \cdot m^{-3}}$] and $\dot{Q}_s$ [$\mathrm{W \cdot m^{-2}}$]. P_{cv} [m], y_b [m], L_c [m], L_{xtot} [m], L_{ztot}[m], L_{ytot}[m] are respectively the perimeters on y and z axis, the contact width, the contact length, the strip length, the strip depth and the strip width. All these variables are represented on Fig. 1.

The catenary grid imposes a stagger motion at a velocity v_{stag} [$\mathrm{m \cdot s^{-1}}$] which is proportional to train velocity V_{train} [$\mathrm{km \cdot h^{-1}}$].

The strip has a particular shape but, owing to the low influence of the bevels on thermal effects, we assume a constant cross section S [$\mathrm{m^2}$].

The surface heat production is allocated along the contact width with a repartition function f_s which characterises the

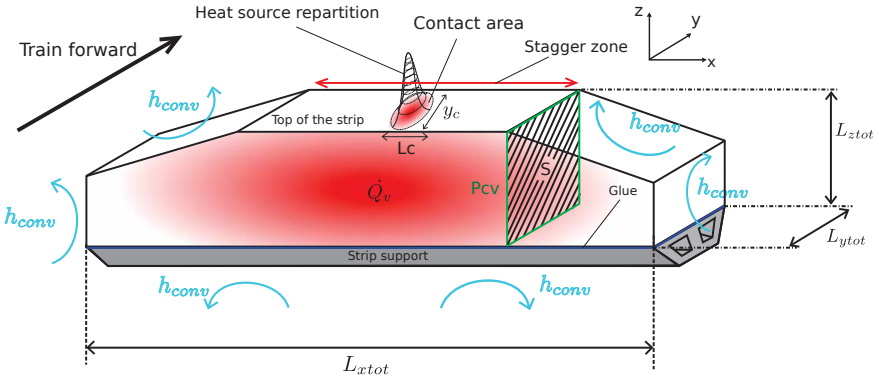

Fig. 1 Pantograph strip description

shape and the quality of the mechanical contact. Notice that, due to the train motion and to the catenary grid staking, the contact area is moving along the x-axis depending on a zig-zag function $\mu(t)$.

III. Modelling

Taking into account the fact that the surface thermal production moves along the x-axis, we will substitute to the formal 3D problem, a system of two PDEs. The first one (1D model) will only consider the evolution along the x-axis, while the second PDE (2D model) will be defined on the cross section *i.e.* in the y, z-plane.

A. 1D Model

The evolution of the temperature T [°C] in a 1D formulation (*i.e.* along the x axis) can be written [10] as follows :

$$\rho C_p \frac{\partial T}{\partial t} = \frac{\partial}{\partial x}\left(k\frac{\partial T}{\partial x}\right) - \frac{hP_{cv}}{S}(T - T_\infty) + \frac{\dot{Q}_s \cdot y_c}{S} + \dot{Q}_v \quad (1)$$

where $\dot{Q}_v$ is the volumetric heat source [$\mathrm{W \cdot m^{-3}}$] and $\dot{Q}_s$ is the surface heat source [$\mathrm{W \cdot m^{-2}}$] defined by :

$$\dot{Q}_s = \tau \cdot f_s(x) \cdot \left(R_{elc} I^2 + F \cdot v_{train} \cdot \mu_f\right) \quad (2)$$

The coefficient μ_f [−] denotes the friction coefficient, R_{elc} [Ω] the electrical contact resistance, I [A] the electric current and F [N] the contact force. Indeed, $\dot{Q}_s$ depends both on the repartition function f_s and on a thermal share coefficient τ given by :

$$\tau = \frac{\left(2 - \sqrt{2}\right) k_{wire} + 2k_{strip}\sqrt{2\pi Pe}}{4k_{wire} + 2k_{strip}\sqrt{2\pi Pe}} \quad (3)$$

According to [9] the coefficient τ is thus a combination of thermal conductivities k_{strip} and k_{wire} of the two materials in contact. The dimensionless number Peclet is defined by $Pe = \frac{v_{stag} L_c}{2\alpha}$ [−] while the thermal diffusivity satisfies $\alpha = \frac{k_{strip}}{C_p \cdot \rho}$ [$\mathrm{m^2 \cdot s^{-1}}$]. Pe could be seen as the capacity of a material in sliding contact with an other to diffuse the heat into itself as a function of the velocity. Notice that (3) is only valid for $Pe > 5$ which corresponds, in our case, to a minimal train velocity of $40\,\mathrm{km \cdot h^{-1}}$. The f_s function is a classical Gaussian distribution which traduces the area of the mechanical contact. The heat production Q_v is computed with Maxwell-Ampere and Ohm's law equations to obtain the electrical field and will not be detailed in here.

The moving surface heat production generates complications for the numerical matrix treatment. So we introduce, as in [4] and [12], a classical mathematical transform.

$$\xi = x - \mu(t) \quad (4)$$

$\mu(t)$ being the position of the catenary along the x-axis. Furthermore, we introduce some more modifications, namely :

$$\begin{aligned} \theta &= T - T_\infty \\ \xi^* &= \frac{\xi + L_s}{2.L_s} \end{aligned} \quad (5)$$

where L_s represents a simulation length longer than the real carbon strip one. These transformations present two main advantages : a motionless contact zone and a fixed domain, namely $[0, 1]$.

Due to the contact area smallness, one has to consider very fine meshes. Moreover, the important train velocity requires very small computation time steps. All this induces high computation times and important computer memory requirements. To overcome this problem, we have considered refined mesh principles, techniques often used (see for instance [16] or [1]). To this purpose, we introduce the following local refined mesh function g_t :

$$\begin{aligned} \xi^* &= g_t(\gamma) \\ \xi^* &= \tfrac{1}{2A}\sinh\left\{p \cdot \left(\gamma - \tfrac{1}{2}\right)\right\} + \tfrac{1}{2} \end{aligned} \quad (6)$$

where $A = \sinh(p/2)$. The p coefficient allows to adapt the mesh at the contact (*i.e.* to the number of points over the contact area).

The final 1D heat equation can be expressed as follows :

$$\rho C_p \left(\frac{\partial \theta}{\partial t} - \frac{1}{2L_S} v_{stag} \cdot D_0(\gamma) \frac{\partial \theta}{\partial \gamma} \right) = \frac{1}{4L_S^2} \left[D_2(\gamma) \frac{\partial}{\partial \gamma} \left(k \frac{\partial \theta}{\partial \gamma} \right) + k \cdot D_1(\gamma) \frac{\partial \theta}{\partial \gamma} \right] - \frac{hP_{cv}}{S} \theta + \frac{\dot{Q}_s \cdot y_c}{S} + \dot{Q}_v \quad (7)$$

The functions D_0, D_1 and D_2 are obtained using (6) and satisfy the following relations :

$$\begin{aligned} D_0(\gamma) &= \frac{\partial \gamma}{\partial \xi^*} = \left(\frac{\partial \xi^*}{\partial \gamma} \right)^{-1} \\ D_1(\gamma) &= - \left(\frac{\partial^2 \xi^*}{\partial \gamma^2} \right) \cdot \left(\frac{\partial \xi^*}{\partial \gamma} \right)^{-3} \\ D_2(\gamma) &= \left(\frac{\partial \xi^*}{\partial \gamma} \right)^{-2} \end{aligned} \quad (8)$$

B. 2D Model

As already mentioned, the 2D model is defined on $y - z$ directions. The related equation writes as :

$$\rho C_p \frac{\partial T}{\partial t} = \frac{\partial}{\partial y} \left(k_y \frac{\partial T}{\partial y} \right) + \frac{\partial}{\partial z} \left(k_z \frac{\partial T}{\partial z} \right) + \dot{Q}_v \quad (9)$$

Taking into account the low dimensions of the domain along these two axes, it isn't necessary to have an important number of nodes. Let us first introduce, like in 1D model, some elementary dimensionless transforms, namely :

$$\begin{aligned} \theta &= T - T_\infty \\ y^* &= y / L_{ytot} \\ z^* &= z / L_{ztot} \end{aligned} \quad (10)$$

The initial PDE (9) becomes :

$$\rho C_p \frac{\partial \theta}{\partial t} = \frac{1}{L_{ytot}^2} \frac{\partial}{\partial y^*} \left(k_y \frac{\partial \theta}{\partial y^*} \right) + \frac{1}{L_{ztot}^2} \frac{\partial}{\partial z^*} \left(k_z \frac{\partial \theta}{\partial z^*} \right) + \dot{Q}_v \quad (11)$$

However, despite a conventional 2D model, the boundary conditions have to be carefully studied.

According to the considered 2D section position, three kinds of boundary conditions occur (see Fig. 4) :

BC3 : Represents the extreme side of the strip. In that position, the convective thermal flux is present on all the mesh. Moreover, the boundaries (sides, bottom and top) of this section are concerned by added convective thermal flux.

BC2 : Represents an internal position everywhere along the strip, except below the contact zone. Convective thermal effects apply on all boundaries in such a situation.

BC1 : Represents a position below the contact zone. The convective thermal fluxes concern the boundaries of the section which are not exactly below the contact area. On the remaining part of the top, a input heat flux coming from the surface heat production must be considered.

The boundary condition BC1 involves a heat production on the top face. Moreover, depending of the considered section position, the number of mesh points concerned by that boundary condition changes.

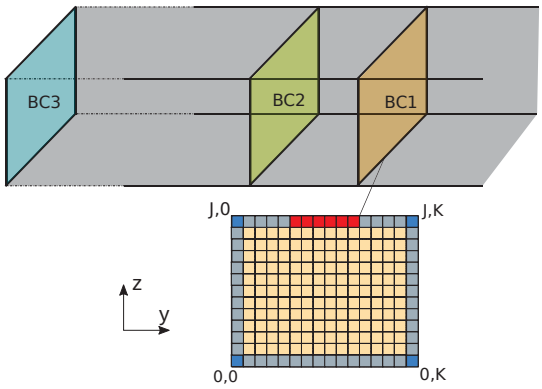

Fig. 2 Boundary conditions of the 2D model in function the simulation position into the strip. The 2D model has a total of $J \times K$ nodes

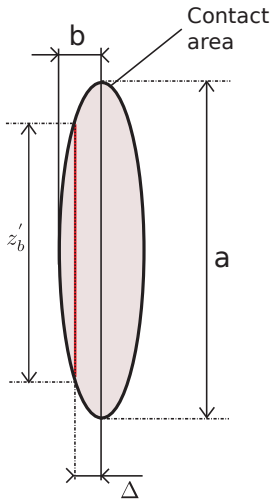

Fig. 3 Representation of the length (z_b') concerned by the surface heat production

We note Δ the distance between the considered section in the 2D model and the contact zone center conforming to the 2D resolution on the 1D mesh point III-C), it is possible to calculate the length z_b' using the following equation :

$$z_b' = a \cdot \sqrt{2 - 8 \cdot \left(\frac{\Delta}{b} \right)^2} \quad (12)$$

For instance, let us analyse more precisely the energy balance method used for the boundary condition in the top right corner (*i.e.* position (0,J)).

The energy conservation equation at this particular point writes :

$$\frac{\partial E}{\partial t} = q_1 + q_2 + q_3 + q_4 + G \quad (13)$$

where q_i represents one of the different thermal fluxes (q_1, q_2 heat conduction and q_3, q_4 convection), E the storage energy

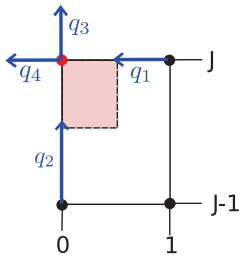

Fig. 4 Energy balance method for a point at (J,0)

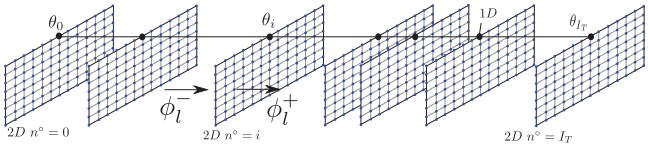

Fig. 5 Representation of a 2.5D configuration. Each cross section could be specified and is labelled by an index i

in the finite volume and G the heat generation. The difference equation becomes :

$$\theta_{J,0}^n = \theta_{J,0}^{n+1} - \frac{\Delta t}{\rho.C_p}\left[\left(\frac{k_y}{L_{ytot}^2}.\frac{2}{\Delta y^2} - \frac{k_z}{L_{ztot}^2}.\frac{2}{\Delta z^2} + \frac{2.h_z}{L_{ytot}.\Delta y} + \frac{2.h_x}{L_{ztot}.\Delta z}\right)\theta_{J,0}^{n+1} + \left(\frac{k_y}{L_{ytot}^2}.\frac{2}{\Delta y^2}\right)\theta_{J-1,0}^{n+1} + \left(\frac{k_z}{L_{ztot}^2}.\frac{2}{\Delta z^2}\right)\theta_{J,1}^{n+1} + \dot{Q}_v\right] \tag{14}$$

C. 2.5D Model

2.5D dimensional modelling methods, also named quasi-3D representation methods, are rarely used in the thermal problems treatment. They have been developed in many other domains, especially when fast computation and low memory requirements are necessary. For example, one can refer to [11] where a 2.5D is used in order to determine the electrical potential on 2D sections and thus to generate a wave modelling.

The first step to create a 2.5D modelling is to simulate the 1D model. We thus obtain the temperature evolution along the x direction (Fig. 1).

To be relevant the 2D model should take into account the heat flux leakage that takes place in the x direction (*i.e.* normal to the cross section S).Thanks to the 1^{st} Fourier's law these fluxes could be computed based on the 1D model results. It is necessary to choose the more significant points for compute a 2D model, and these point positions (i index from 0 to I_T) can be found using criteria on temperature gradient. If we note $\phi_l^{\pm}$ these fluxes, we can express them as follows :

$$\phi_l^{\pm} = -k_x.S.\frac{\partial\theta}{\partial x}|_{i^{\pm}} = -\frac{k_x.S}{2.L_S}.D_0(\gamma).\frac{\partial\theta}{\partial\gamma}|_{i^{\pm}} \tag{15}$$

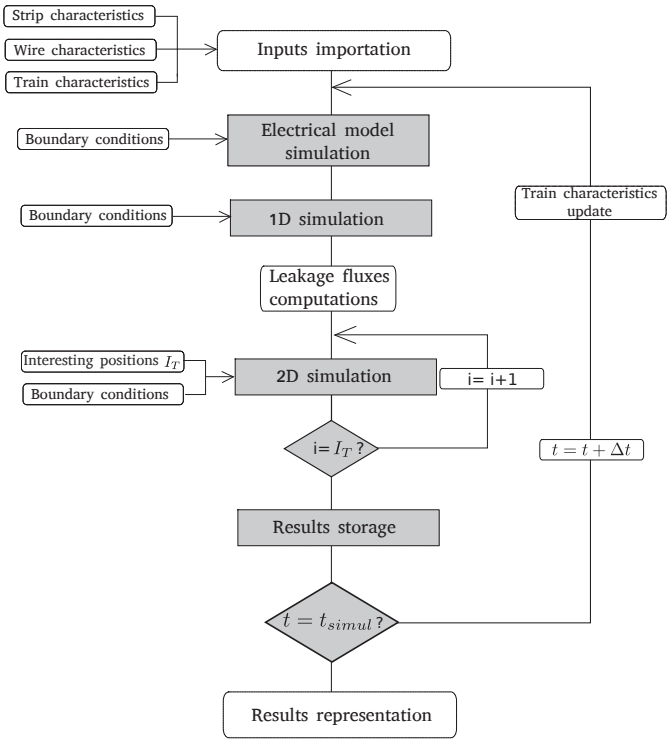

Fig. 6 Coding organizational chart

The notation $\phi_l^{\pm}$ refers to heat leakage coming from the left at the position i (*i.e.* i^-) or the one leaving to right (*i.e.* i^+) (Fig. 5). Using this relation together with classical discretisation for a considered point inside the domain (position j, o), (11) becomes :

$$\theta_{j,o}^n = \theta_{j,o}^{n+1} + \frac{\Delta t}{\rho.C_p}\left[\theta_{j,o}^{n+1}\left(\frac{2.k_z}{\Delta z^2} + \frac{2.k_y}{\Delta y^2}\right) + \theta_{j+1,o}^{n+1}\left(-\frac{k_z}{\Delta z^2}\right) + \theta_{j,o+1}^{n+1}\left(-\frac{k_y}{\Delta y^2}\right) + \theta_{j-1,o}^{n+1}\left(-\frac{k_z}{\Delta z^2}\right) + \theta_{j,o-1}^{n+1}\left(-\frac{k_y}{\Delta y^2}\right) + \dot{Q}_v - \frac{\phi_l^+}{\Delta x.S_{j,o}} + \frac{\phi_l^-}{\Delta x.S_{j,o}}\right] \tag{16}$$

The quantity Δx corresponds to the width of the considered cross section . However, the 2D positions (i) can be located between two mesh points. To overcome this problem, the leakage fluxes are interpolated along the 1D model.

To conclude, we can summarize our whole 2.5D model by the following organizational chart

IV. Experimental Device

A. Strip Configuration

Nineteen thermocouples have been inserted inside the carbon strip at specific positions described on Fig. 7. They were maintained by a thermal glue to prevent them from any air-gap. The signals emitted by the thermocouples were acquired at a frequency of $60Hz$.

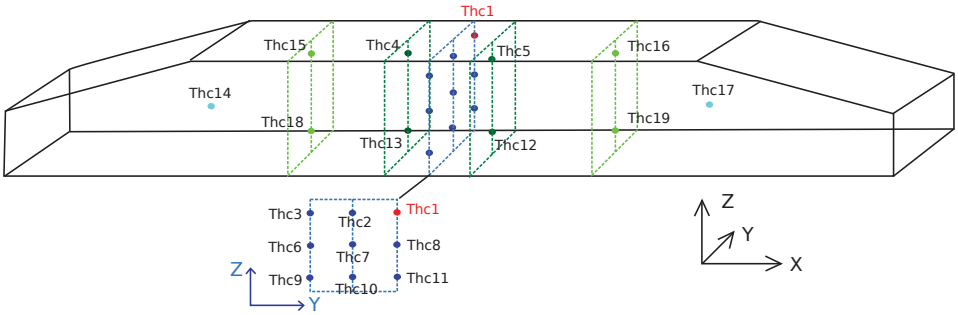

Fig. 7 Arrangement of thermocouples in the pantograph strip

Many entry parameters have been tested, especially the train velocity, the electrical current, the contact force and the stagger amplitude :

- Three velocity : Variable (Fig. 8)-140-180km $\cdot$ h^{-1}
- Two contact forces : 60-90N
- Three currant steps : 300-500-700A
- Two catenary grid configurations

Fig. 8 highlighted the input parameters for a variable velocity, a normal current profile and a fixed catenary grid configuration.

B. Test Bench and Experimental Setup

The test bench we used is able to reproduce the current collection configurations between a strip and a contact wire for a moving train (Fig. 9). For a complete description, one can refer to [8] and [5].

This test bench presents some particularities which have to be considered. For instance, the ventilation equipment as a width corresponding to 1/3 of the strip width, so only a third part of the strip is cooled by forced convection. Moreover, during the tests, the strip was often laterally leaned due to its weight. Therefore, the contact area did shift along the strip width. We did take into account various inputs parameters such as the electrical current, voltage, contact force, stagger amplitude and velocity, airflow velocity and train velocity. These inputs were acquired and filtered to use them into the model. The results obtained by the thermocouples have been treated for a better visibility.

V. Result and Discuss

Comparisons between theoretical and experimental results are quite hard to study because of the number of inputs which are unknown, namely :

- The contact area which directly defines the electrical contact resistance and so, the surface heat source.
- None measures of the real convective coefficients have been realised ; a CFD simulation has allowed to obtain them.
- The thermal conductivity is particularly difficult to obtained and its evolution in relation to the strip wear is unknown.

Moreover, the experimental setup is limited because of the thermocouples placed inside the strip. The contact area has a small width so the distance between the thermocouples doesn't allow a strictly local thermal representation.

The matter used is one of the most important parameters for the simulation. Indeed, the thermal conductivity of the used matter will characterise the cooling *i.e* the thermal exchange between the surface, the fluid and by association, the Biot number ($Bi = \frac{h.L_c}{k}$).

A. 1D Results and Comparison

The first thermal step of the model, according to Fig. 6, is to compute the 1D model. It gives some interesting results :

The electric power injected into the strip has a incontestable effect on its temperature, the two thermal sources depending upon electrical data. Experimental and simulation results present a similar behaviour. We note a 8,5% error rate for the first current step, 7,8% for the second and 20,8% for the third. These errors can be explained by the fact that the convective model results are directly compared to thermocouples which are inside the matter. Moreover, thermal values obtained by simulation are lower than experimental results. This can be considered as a consequence of the bench airflow equipment which isn't really representative of a real train situation (IV-B). For instance, when the contact zone is located at an extreme side of the stagger zone, an important part of the strip isn't cooled. On the other hand, one can see that, after around 7 min, a singular thermal peak on experimental results : it is due to electrical arcs. For the moment, our model doesn't take into account such phenomena.

Fig. 11 shows simulation and theoretical responses in a variable velocity case. A serious thermal overheating can be seen. This phenomenon is correctly anticipated by the model, but with lowest temperature as a consequence of a better cooling. This is a typical behaviour of second order thermal PDE. Depending on the convective factor, cooling or heating diffuses quickly in the strip. But, as previously said, this factor is unknown, and its estimation not optimum. From a general point of view and by comparison to Fig. 10, it can be noted, as in the black square, very similar stagger effects. However, there is a higher temperature difference in the variable velocity case. In fact, in that last situation, many vibrations appear and induce electrical arcs such as in the red square. The important number of electrical arcs also testifies bad quality of the contact zone. Emphasised temperature errors can thus be

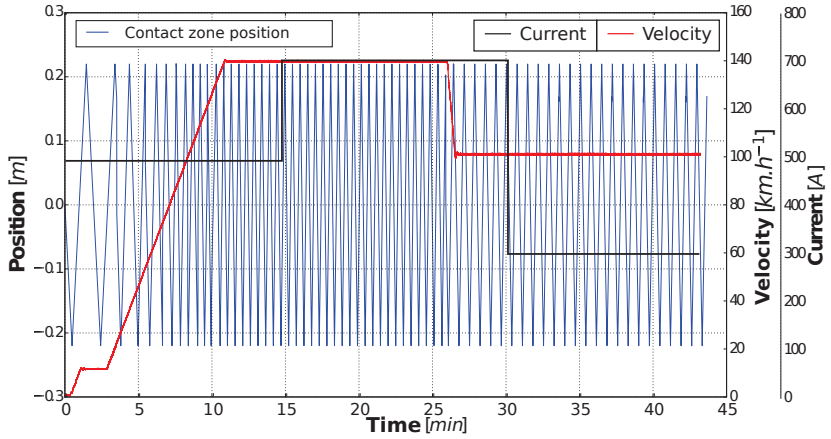

Fig. 8 Input train velocity, equivalent stagger position of the contact zone on the pantograph strip length and electrical current

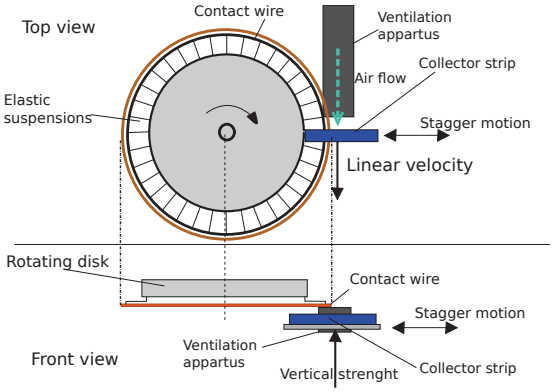

Fig. 9 Representation of the experimental bench

attributed to the difference between our theoretical contact area value and the real one, parameter which defines directly the surface heat source. Finally, notice that, this variable profile with a low velocity associated with a high current at the beginning is specific of a train start. In the yellow square, we can see thermal peaks which could be damageable for the pantograph strip.

Moreover, there is an other parameter which has an important influence on the strip thermal phenomena, it is the frequency of the contact presence above a fixed position. The experimental setup doesn't allow representing this phenomenon in 2D because of the low thermocouples number elsewhere except center. The model highlights it, especially in 1D :

The stagger thermal effect is most important because of the presence time of the contact zone above the observed zone. This zone has a higher time far from the contact area and so far from the surface heat source and it can have a better cooling.

B. 2D Experimental Results

Fig. 13 shows the experimental thermal distribution in the middle of the strip. The temperature reaches a maximum value of 179°C on the top and a temperature of 88.89°C on the bottom. These two values represent the most important results for industrial issues I. The first observation is the off-centered position of the heat spot : this is significant of a contact area located at a side of the 2D domain y, z. Further simulations will be made with similar conditions. This heat source position can be explained by the convection shape. The CFD simulation realized (Fig. 15) shows a large difference between the convective coefficients in function of the considered faces.

An other parameter can also explained this heat spot placement : it is the material characteristics such as the thermal conductivity. The considered carbon is a hugely anisotropic material. Therefore, the thermal conductivity is most important along the y axis than z axis. This induces a temperature increase on one side.

C. Classical Simulation

For a classical simulation, the surface heat flux is placed at the middle of the 2D model top.

The temperature diffuses into the material, diffusion being more important on one side according to comments made about conductivity. We can note the influence of the different values of the convective coefficient in function of faces. Indeed, the temperature value on the right side is lower than on the other side. The surface temperature reaches a maximum value of 162°C If we consider the averaged temperature on the domain at a fixed point, it confirms by comparison to the averaged value obtained with the 1D model (see Fig. 16), the 2.5D model validity. Notice that the 2D average temperature is given by :

$$T_a = \sum_{c=0}^{J*K} \left(\frac{S_c}{S} . T_{2D} \right) \tag{17}$$

D. Compared Simulations

For situations with data described in Fig. 13, the model gives the following results :

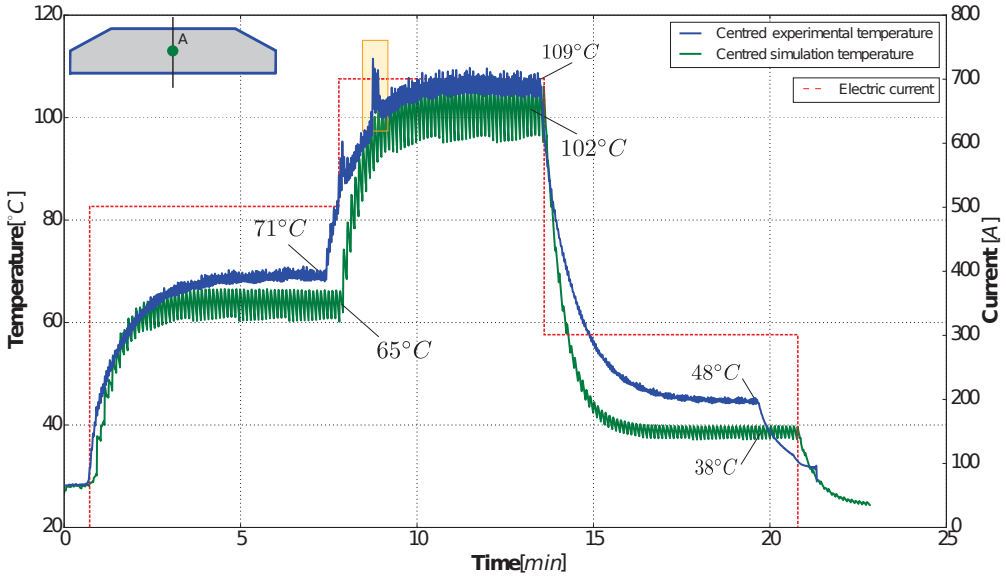

Fig. 10 Representation of the 1D temperature for a 1D model, a constant velocity at 140km · h^{-1}, three current steps, a contact force of 60N and a normal stagger motion

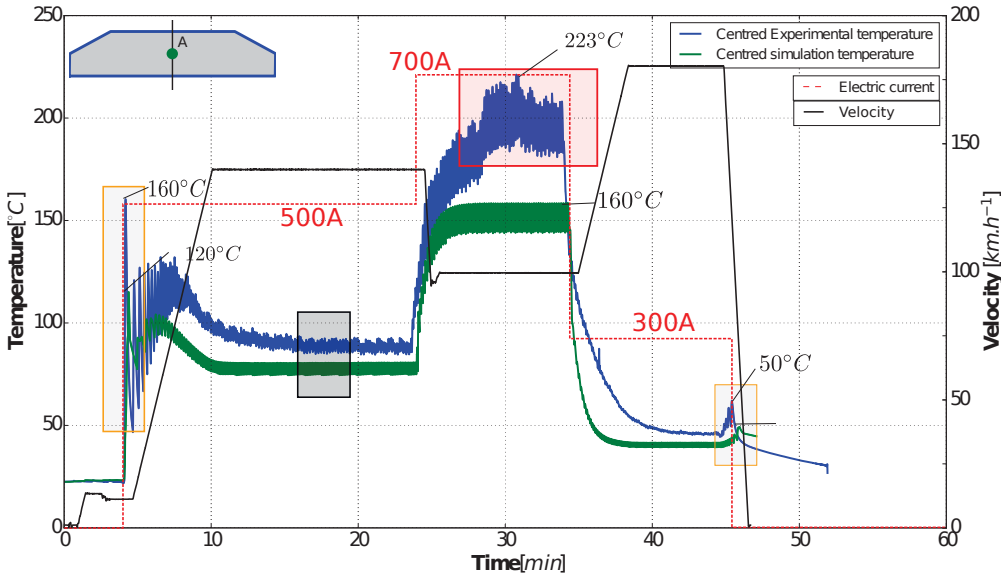

Fig. 11 Representation of the 1D temperature for a 1D model, a variable velocity, three current steps, a contact force of 90N and a normal stagger motion

We have a similar thermal repartition : the maximum temperature is quite the same, however the impact of thermal convection is most important in the experimental case. It is probably due to the fact that thermal conductivity values aren't really optimal.

Despite some differences, the model gives some good and promising results. Thus, it can be used to characterise the strip temperature evolution.

E. Simulation Observations

Next figures represent three 2D cross-sections : one is located at the contact zone ($x = 0$) while the two others are on both sides. They are all separated by 1cm. The motion direction is opposite of x axis (see Fig. 1). As the three positions are roughly at the "center" of the strip, the conductivity along the x axis will be supposed constant.

On Fig. 18, the temperature is quite constant over the domain, the only heat source acting here being the volume heat production.

On Fig. 19, the temperature is maximal, since we are exactly below the contact area. However, the temperature hasn't diffused into the material.

This last figure is interesting because the considered position is symmetric, with respect to contact zone location, to position

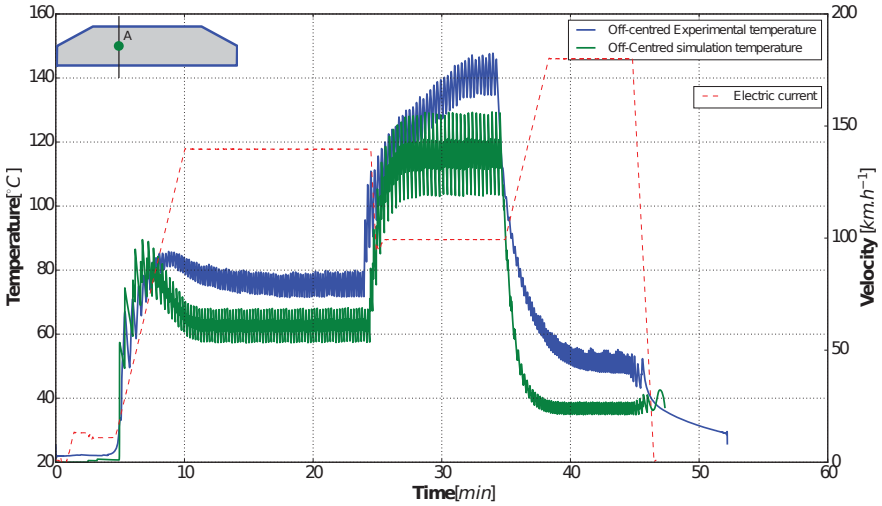

Fig. 12 Temperature of an off-center position by 20cm in 1D for a variable profile

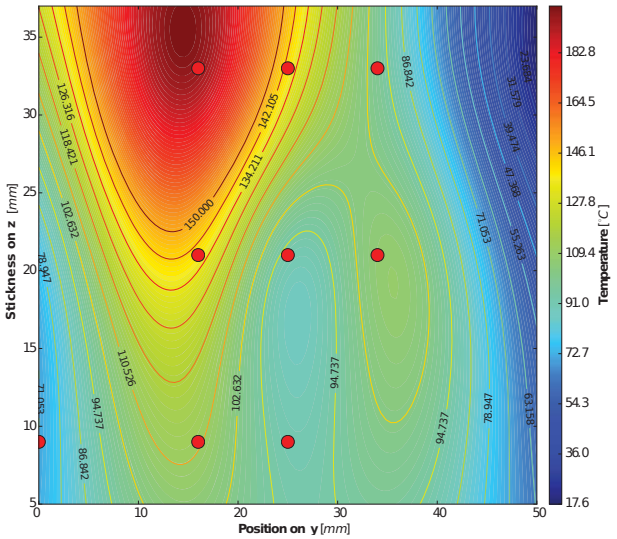

Fig. 13 Experimental 2D interpolated results between the transversal thermocouples on Z,Y at 100s of simulation for a current of 500A, a velocity of 140km $\cdot$ h^{-1} a,f a force of 60N

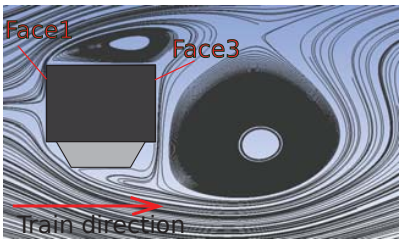

Fig. 14 CFD simulation for same configuration than in Fig. 13, Face 1 : forward motion. Face 3 backward motion

defined in Fig. 18. However, we can observe a large difference between those two thermal distributions. It is due to Peclet number. Indeed, the high stagger velocity induces an important

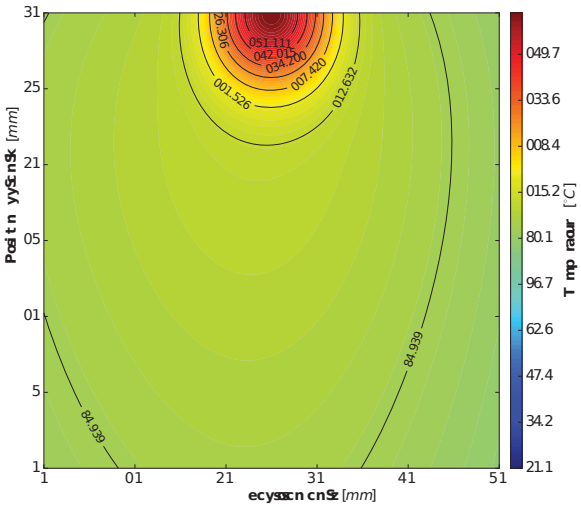

Fig. 15 2D simulation results of the model for the same configuration than Fig. 13 but with a surface heat source centred

Peclet number. Therefore, temperature is highly diffused in the opposite motion direction, while presents a particularly brutal front in train movement direction.

On Fig. 21, the thermal effect of a high Peclet number is highlighted.

We observe the very low temperature of the domain at the x position -3, but in the opposite of move direction, we have a thermal distribution more important. Theses principles are described in [12].

VI. Conclusion

- The 2.5D method proposed in this paper allows characterising the strip temperature in all directions without the use of 3D simulation. Computation time and memory requirement are significant for an equivalent accuracy. The link between the 1D and 2D models via

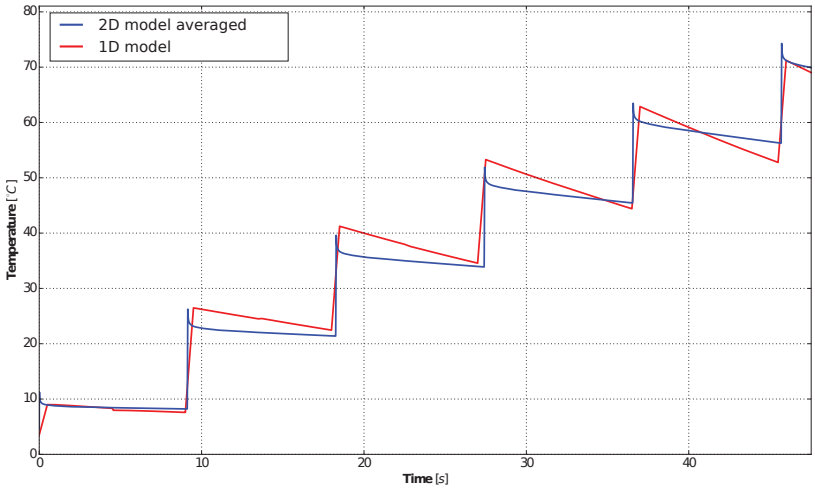

Fig. 16 The 2D averaged temperature compared to the 1D temperature for a first step of numerical validation of the temperature computations

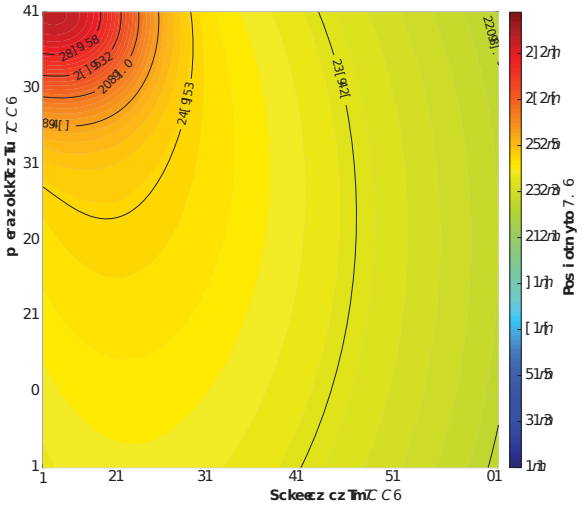

Fig. 17 2D simulation results of the model for the same configuration than Fig. 13

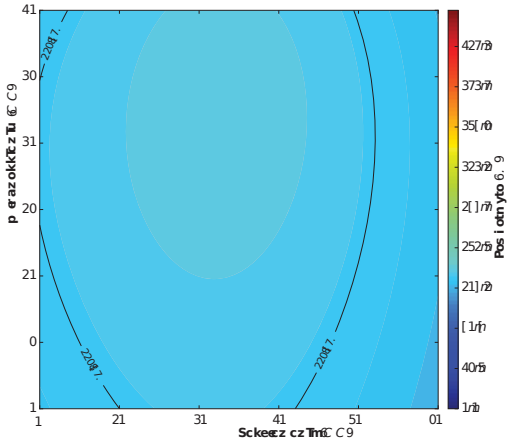

Fig. 18 Position B off-centred of 1cm in motion direction at 450s of simulation for a electrical current of 700A

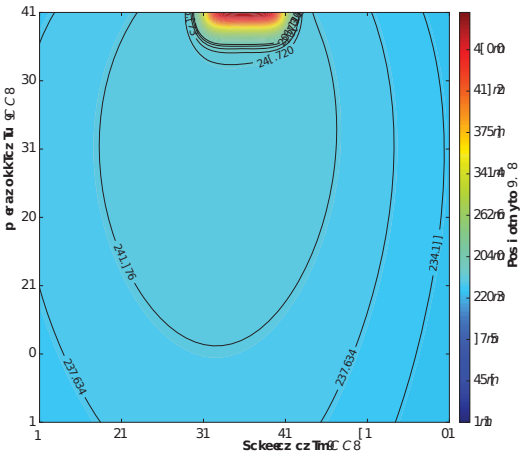

Fig. 19 Position A centred on 0 at 450s of simulation for a electrical current of 700A

the leakage fluxes permits to conserve all thermal effects such as a 3D simulation.

- Despite some unknowns parameters, the results allow studding many thermal effects like the influence of the stagger motion, the thermal distribution inside the material, the convection influence and particularly the effects of links between all the inputs parameters.
- The results obtained with the 2.5D strategy show many interesting thermal elements. Taking into account the high proximity between experimental and simulation results for many thermal phenomena, we can consider that, in many cases, the model can traduce the thermal evolution of the strip for a moving train.
- It is difficult to treat here all the phenomena intervening during a real train trip. However this paper, highlights some of the most important thanks to a complex model. Further studies will complete this realised work with

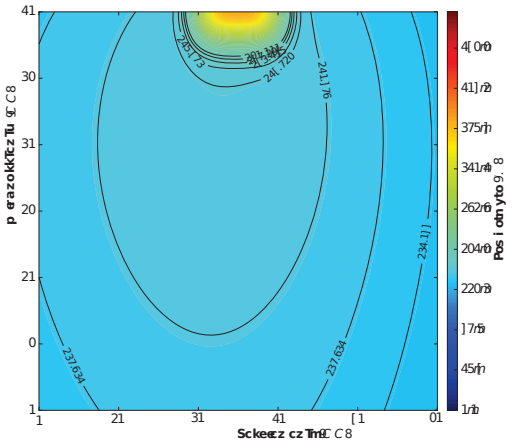

Fig. 20 Position C off-centred of 1cm in opposite motion direction at 450s of simulation for a electrical current of 700A

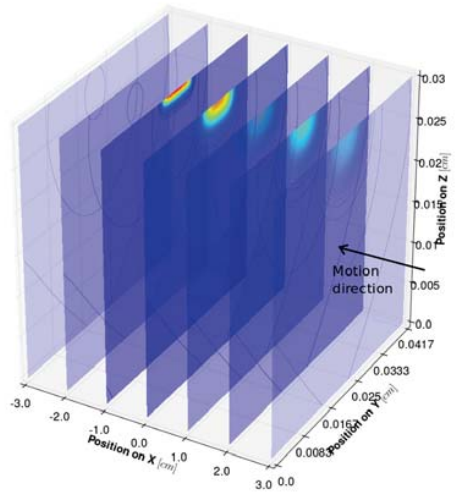

Fig. 21 Position B off-centred of 1cm in motion direction at 450s of simulation for a electrical current of 700A

more accurate inputs values such as for the contact area, the conductivity coefficient and so on.

REFERENCES

[1] JD Anderson Jr. *Transformations and Grids*. Springer, 2009.

[2] M. Braunovic, V. Konchits, and N. K. Myshkin. *Fundamentals of Electrical Contacts*. Applications and Technology, 2006.

[3] C. Tu, Z. Chen, and J. Xia. Thermal wear and electrical sliding wear behaviors of the polyimide modified polymer-matrix pantograph contact strip. *Elsevier : Tribology*, Volume 42 :995–1003, 2009.

[4] D. Rosenthal. The theory of moving sources of heat and its application to metal treatement. In *ASME Trans.*, pages 849–866, 1946.

[5] E. Fedeli, R. Manigrasso, G. Bucca, and A. Collina. Interactions between the quality of pantograph current collection and the codified current signalling. *IMechE*, 225, 2008.

[6] F. P. Incropera, D. P. Dewitt, T. L. Bergman, and A. S. Lavine. *Fundamentals of Heat and Mass Transfer*. 2013.

[7] Pengzhao Gao, Hongjie Wang, and Zhihao Jin. Study of oxidation properties and decomposition kinetics of three-dimensional (3-d) braided carbon fiber. *Thermochim Acta*, 414 :59–63, 2004.

[8] G. Bucca and A. Collina. A procedure for the wear prediction of collector strip and contact wire in pantograph-catenary system. *Elsevier : Wear*, Volume 266 :46–59, 2009.

[9] H. Block. Theoretical study of temperature rise at surfaces of actual contact under oiliness lubricating conditions. In Institution of Mechanical Engineers, editor, *Proceedings of the General Discussion on Lubrication and Lubricants*, pages 222–235. London, The Institution, 1938.

[10] H. S. Carslaw and J. C. Jeager. *Conduction of heat in solids*. Oxford University, 1959.

[11] Zhang Qian-Jiang, Dai Shi-Kun, Chen Long-Wei, Qiang Jian-Ke, Li Kun, and Zhao Dong-Dong. Finite element numerical simulation of 2.5d direct current method based on mesh refinement and recoarsement. *Applied geophysics*, 13(2) :257–266, 2016.

[12] R. Weichert and K. Schonert. Temperature distribution produced bu a moving heat source. *The Quarterly Journal of Mechanics and Applied Mathematics*, pages 363–379, 1978.

[13] S. Kubo and H. Tsuchiya. Wear properties of metal-impregnated carbon fiber-reinforced carbon composite sliding against a copper plate under an electrical current. In *World Tribology Congress III*, number Institute, 2005.

[14] T. Bausseron. *Etude de l'échauffement de la catenaire lors du captage a l'arrêt*. PhD thesis, Universite de Franche-comte, 2014.

[15] T. Ding, G. X. Chen, J. Bu, and W. H. Zhang. Effect of temperature and arc discharge on friction and wear behaviours of carbon strip/copper contact wire in pantograph-catenary systems. *Elsevier : Wear*, Volume 271 :1629–1636, 2011.

[16] T. Hoist. Numerical solution of axisymmetric boattail fields with plume simulator. *AIAA Paper*, pages 77–124, 1977.

[17] Ales Turel, Janko Slavic, and Miha Boltezar. Electrical contact resistance and wear of a dynamically excited metal? ? ?graphite brush. *Advances in Mechanical Engineering*, 9 :1–8, 2017.